Tm,Ho:Ca(Gd,Lu)AlO4 crystals: Polarized spectroscopy and laser operation

Zhongben Pan, Pavel Loiko, Josep Maria Serres, Hualei Yuan, Yicheng Wang, Li Wang, Yongguang Zhao, Rosa Maria Solé, Magdalena Aguiló, Francesc Díaz, et al.

Journal of Luminescence 257 (2023) 119638

Contents lists available at ScienceDirect

Journal of Luminescence

journal homepage: www.elsevier.com/locate/jlumin

Full Length Article

Tm,Ho:Ca(Gd,Lu)AlO_4 crystals: Polarized spectroscopy and laser operation

Zhongben Pan [a,b], Pavel Loiko [c], Josep Maria Serres [d,e], Hualei Yuan [f], Yicheng Wang [b], Li Wang [b], Yongguang Zhao [b,g], Rosa Maria Solé [d], Magdalena Aguiló [d], Francesc Díaz [d], Patrice Camy [c], Weidong Chen [b,h], Uwe Griebner [b], Valentin Petrov [b], Xavier Mateos [d,1,*]

[a] School of Information Science and Engineering, Shandong University, Qingdao, 266237, China
[b] Max Born Institute for Nonlinear Optics and Short Pulse Spectroscopy, Max-Born-Str. 2a,12489, Berlin, Germany
[c] Centre de Recherche sur Les Ions, Les Matériaux et La Photonique (CIMAP), UMR 6252 CEA-CNRS-ENSICAEN, Université de Caen Normandie, 6 Boulevard Du Maréchal Juin, 14050 Caen Cedex 4, France
[d] Universitat Rovira I Virgili, Fisica I Cristal·lografia de Materials I Nanomaterials, FiCMA-FiCNA, 43007, Tarragona, Spain
[e] Eurecat, Centre Tecnològic de Catalunya, Advanced Manufacturing Systems Unit (AMS), Marcel·lí Domingo 2, 43007, Tarragona, Spain
[f] Institute of Chemical Materials, China Academy of Engineering Physics, Mianyang, 621900, China
[g] Jiangsu Key Laboratory of Advanced Laser Materials and Devices, Jiangsu Normal University, 221116, Xuzhou, China
[h] Key Laboratory of Optoelectronic Materials Chemistry and Physics, Fujian Institute of Research on the Structure of Matter, Chinese Academy of Sciences, Fuzhou, 350002, Fujian, China

ARTICLE INFO

Keywords:
Aluminate crystals
Holmium ions
Absorption
Stimulated emission
Luminescence decay
Laser operation

ABSTRACT

Tm^{3+},Ho^{3+}-codoped and compositionally "mixed" disordered Ca(Ga,Lu)AlO_4 aluminate crystals are promising materials for ultrashort pulse generation above 2 μm. Their polarized spectroscopic properties are studied and the effect of Lu^{3+} codoping on the inhomogeneous spectral broadening is verified. The peak stimulated-emission cross-section for the $^5I_7 \rightarrow {}^5I_8$ Ho^{3+} transition is 1.05×10^{-20} cm^2 at 2000 nm for π-polarization. The $Tm^{3+} \leftrightarrow Ho^{3+}$ energy-transfer parameters are $P_{28} = 1.42$ and $P_{71} = 0.090$ [10^{-22} $cm^3 \mu s^{-1}$] indicating a direct transfer with a thermal equilibrium time of 4.35 ms. The effective gain spectra for the codoped crystal are derived. For σ-polarization, the gain bandwidth at ~2.04 μm is about 100 nm; particularly for this light polarization, Lu^{3+} codoping induces a noticeable red-shift of the emission spectra further beyond 2 μm. Using absorption studies at 12 K, the Stark splitting of the Tm^{3+} and Ho^{3+} multiplets is resolved. A laser-pumped Tm,Ho:Ca(Ga,Lu)AlO_4 laser generated a maximum output power of 763 mW at 2078.6 nm with a slope efficiency of 26.4% and π-polarized emission. A continuous wavelength tuning between 1887.7 and 2127 nm (tuning range: 239.3 nm) was achieved for *σ*-polarization. Diode-pumped operation of ***a***-cut and ***c***-cut crystals was also studied.

1. Introduction

Holmium ions (Ho^{3+}) are known for broadband eye-safe emission at wavelengths slightly above 2 μm owing to the $^5I_7 \rightarrow {}^5I_8$ electronic transition [1]. Ho lasers find applications in atmospheric remote sensing, range-finding (LIDAR), wind mapping and surgery [2,3]. Due to the typically long upper laser level ($^5I_7$) lifetime, Ho lasers exhibit good energy storage capabilities attaining high pulse energies [4]. They are also suitable as pump sources of mid-IR optical parametric oscillators based on non-oxide nonlinear crystals [5].

A widely used scheme for excitation of Ho^{3+} ions is the codoping with thulium ions (Tm^{3+}) [6–8], pumping them at ~0.8 μm (into the $^3H_4$ multiplet), e.g., using commercial high power AlGaAs laser diodes and subsequent energy-transfer between the $^3F_4$ Tm^{3+} and $^5I_7$ Ho^{3+} multiplets that are resonant in energy. By selecting proper doping concentrations and Tm^{3+}/Ho^{3+} codoping ratio, it is feasible to reach relatively high slope efficiencies. Physically, this involves efficient cross-relaxation (self-quenching) for adjacent Tm^{3+} ions depopulating the $^3H_4$ pump level, as well as predominantly unidirectional $Tm^{3+} \rightarrow Ho^{3+}$ energy transfer (ET) [9]. Loiko et al. reported on a continuous-wave (CW) diode-pumped Tm, Ho laser generating 451 mW at 2081 nm with a slope efficiency of 31% [8].

The main drawback of Tm^{3+},Ho^{3+}-codoped materials is a significant heat loading caused by energy-transfer upconversion (ETU) [7,10] from

* Corresponding author.
E-mail address: xavier.mateos@urv.cat (X. Mateos).
[1] Serra Húnter Fellow.

https://doi.org/10.1016/j.jlumin.2022.119638
Received 7 June 2021; Received in revised form 6 January 2022; Accepted 24 December 2022
Available online 30 December 2022

the metastable states of both active ions. Consequently, for the development of Tm, Ho lasers, it is desirable to employ host materials with a combination of good spectroscopic and thermo-mechanical properties.

Laser materials (crystals) codoped with Tm^{3+} and Ho^{3+} ions are attractive for broadly tunable and especially mode-locked (ML) lasers. This is because the codoping allows one to combine (at least, partially) the gain bandwidths of both active ions. On the other hand, the selection of Ho^{3+} laser transition at >2 μm is preferable to avoid the structured water vapor absorption in the atmosphere which is detrimental for stable mode-locking. Recently, a great progress was achieved in the field of passively mode-locked bulk Tm, Ho lasers [11–13] leading to the generation of ultrashort (sub-100 fs) pulses. Zhao et al. reported on a Tm, Ho laser based on a disordered garnet delivering 79 fs pulses at a central wavelength of 2083 nm (emission bandwidth: 71 nm) at a repetition rate of 99.3 MHz [13]. One of the reasons for such progress is the use of disordered laser materials.

Among the laser host materials suitable for Tm^{3+} and Ho^{3+} doping, calcium rare-earth aluminates $CaLnAlO_4$ (where Ln = Gd [14,15] or Y [16–18]) are attracting especial attention. They exhibit disorder in the crystalline structure (the Ca^{2+} and Ln^{3+} cations are statistically distributed over the same site) [19] leading to significant inhomogeneous broadening of the absorption and emission bands of the rare-earth ions [20], together with attractive thermo-optical properties [21]. CW and ML lasers based on singly Tm^{3+}- [14,17] and Ho^{3+}-doped [18] and Tm^{3+},Ho^{3+}-codoped [11,22] $CaLnAlO_4$ aluminate crystals were reported. Zhao et al. developed a Tm,Ho:$CaYAlO_4$ laser passively mode-locked by a GaSb-based semiconductor saturable absorber mirror and generating 87 fs pulses at 2043 nm; in the CW regime, a continuous wavelength tuning between 1970 and 2085 nm was achieved [11].

A way to improve the broadband emission properties of $CaLnAlO_4$ crystals is to use compositional disorder in $CaLn1_{1-x}Ln2_xAlO_4$ solid solutions. Recently, the spectroscopic and laser properties of Ca(Gd,Lu)AlO_4 crystals doped with Yb^{3+} [23] and Tm^{3+} [24] ions were studied. In the present work, we report on a detailed spectroscopic study and CW laser operation of Tm,Ho:Ca(Gd,Lu)AlO_4 crystals. In the parallel paper [25], we have described the growth, structure, Raman spectra and transition intensities of Ho^{3+} ions in these crystals.

2. Experimental

The Tm,Ho:Ca(Gd,Lu)AlO_4 crystals were grown by the Czochralski (Cz) method, see Ref. [25]for more details. Two crystal compositions with different Lu^{3+} doping (5.5 and 10.8 at.%) were studied corresponding to the stoichiometric chemical formulas $CaGd_{0.8947}Lu_{0.0551}Tm_{0.0448}Ho_{0.0054}AlO_4$ and $CaGd_{0.8432}Lu_{0.1080}Tm_{0.0450}Ho_{0.0038}AlO_4$ referred below as compositions #1 and #2, respectively. Both crystals were oriented along [100] and [001] crystallographic axes. The obvious difference in the actual Ho^{3+} doping level can be due to two reasons: (i) the intrinsic error of the used measurement method, i.e., Inductively Coupled Plasma Mass Spectrometry (ICP-MS), which becomes significant especially for low doping levels; (ii) a gradient of dopant concentration along the crystal growth direction. In the present study, the two Tm,Ho:Ca(Gd,Lu)AlO_4 crystals with different Lu^{3+} contents had different crystal habits due to the unsteady growth condition [25]. Thus, we believe that the difference in the actual Ho^{3+} doping level mainly originates from cutting the crystal samples from different parts of the two boules.

First, the spectroscopic studies were carried out at room temperature (RT, 20 °C). To measure the polarized absorption spectra, a Varian CARY 5000 spectrophotometer equipped with a Glan-Taylor polarizer was used; the spectral bandwidth (SBW) was 0.2 nm. The near-IR luminescence spectra were recorded using an optical spectrum analyzer (OSA, model AQ6375B, Yokogawa, with SBW = 0.1 nm) and a Glan-Taylor polarizer. The set-up was calibrated using a 20 W halogen lamp with a spectrally calibrated emission. The excitation was from a Ti:Sapphire laser (model 3900 S, SpectraPhysics) tuned to 797 nm.

For the measurements of the low-temperature (LT, 12 K) absorption and luminescence spectra, the sample was mounted on an APD DE-202 closed-cycle cryo-cooler equipped with an APD HC 2 Helium vacuum cryo-compressor and a Lakeshore 330 temperature controller.

The luminescence decay studies were realized by means of a ns optical parametric oscillator (OPO, model Horizon, Continuum) and the detection system containing a 1/4-m monochromator (Oriel 77,200), an InGaAs detector and an 8-GHz digital oscilloscope (DSA70804B, Tektronix). The crystals were finely powdered to reduce effect of reabsorption (radiation trapping) on the measured lifetimes [26].

3. Spectroscopic study

3.1. Absorption and luminescence spectra

The absorption spectrum of the Tm,Ho:Ca(Gd,Lu)AlO_4 crystal was analyzed in detail in Ref. [25]. The transition intensities for Tm^{3+} [24] and Ho^{3+} [25] ions were calculated by means of the Judd-Ofelt theory. Here, we will focus on the transition cross-sections and the effect of Lu^{3+} codoping on the absorption and emission bandwidths.

The tetragonal Ca(Gd,Lu)AlO_4 crystal is optically uniaxial (the optical axis is parallel to the ***c***-axis). Thus, there exist two principal light polarizations, $\boldsymbol{E} \,||\, \boldsymbol{c}$ (π) and $\boldsymbol{E} \perp \boldsymbol{c}$ (σ) with the corresponding refractive indices n_e and n_o. For the parent compound, $CaGdAlO_4$, $n_e > n_o$ (optically positive uniaxial crystal) [27]. The spectroscopic properties were measured using ***a***-cut crystals giving access to both principal light polarizations.

In Fig. 1(a), we focused on the absorption bands related to the $^3H_6 \rightarrow {}^3H_4$ and $^3H_6 \rightarrow {}^3F_4$ Tm^{3+} and $^5I_8 \rightarrow {}^5I_7$ Ho^{3+} transitions which are of interest for ~2 μm laser operation. The spectra were measured at RT with polarized light. The absorption spectra for both ions are smooth and broad revealing a "glassy-like" spectroscopic behavior. This is due to the strong inhomogeneous broadening of the spectral lines in the Ca(Gd,

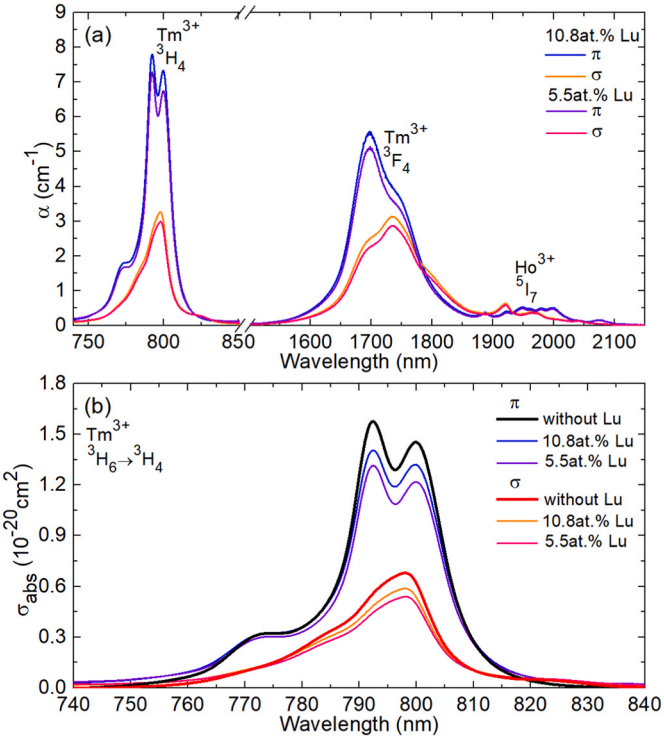

Fig. 1. (a) Absorption bands corresponding to the $^3H_6 \rightarrow {}^3H_4$ and $^3H_6 \rightarrow {}^3F_4$ Tm^{3+} and $^5I_8 \rightarrow {}^5I_7$ Ho^{3+} transitions in Ca(Gd,Lu)AlO_4 crystals with different Lu^{3+} content; (b) absorption cross-sections, σ_{abs}, for the $^3H_6 \rightarrow {}^3H_4$ Tm^{3+} transition (the data for a Tm,Ho:$CaGdAlO_4$ crystal are given for comparison). The light polarizations are π and σ.

Lu)AlO_4 crystals exhibiting both the structure disorder (inherent to $CaLnAlO_4$ compounds) and compositional disorder (due to the addition of Lu^{3+} ions further modifying the multi-ligands around the active ions).

In Fig. 1(b), we calculated the absorption cross-sections, $\sigma_{abs} = \alpha_{abs}/N_{Tm}$, for the $^3H_6 \rightarrow {}^3H_4$ Tm^{3+} pump transition. Here, α_{abs} is the directly measured absorption coefficient and N_{Tm} is the actual Tm^{3+} ion density in the crystal measured by Inductively Coupled Plasma Mass Spectrometry (see Ref. [25]). For the crystal compositions #1 and #2, it was nearly the same, $N_{Tm} = 5.55 \times 10^{20}$ cm^{-3}. In the same figure, for comparison, we provide the σ_{abs} spectra for Tm^{3+} ions in the $CaGdAlO_4$ crystal [24].

For the crystal with the maximum Lu^{3+} content of 10.8 at.% (composition #2), the maximum absorption cross-section σ_{abs} is 1.40×10^{-20} cm^3 at 792.4 nm for π-polarization and the corresponding absorption bandwidth (full width at half maximum, FWHM) $\Delta\lambda_{abs}$ is 18.0 nm. For σ-polarization, the peak σ_{abs} is smaller, namely 0.59×10^{-20} cm^3 at 798.0 nm and $\Delta\lambda_{abs}$ is only slightly broader, 19.4 nm. As compared to the crystal without Lu^{3+} codoping, the polarization-anisotropy of absorption cross-sections is well preserved. Simultaneously, the absolute values of σ_{abs} are reduced. The latter can be in part referred to the error in the N_{Tm} determination. Lu^{3+} codoping induces a slight broadening of the $^3H_6 \rightarrow {}^3H_4$ absorption band for Tm^{3+} ions: for the $CaGdAlO_4$ crystal, the corresponding absorption bandwidths are 16.3 nm (π) and 18.1 nm (σ).

The RT polarized luminescence spectra of the Tm,Ho:Ca(Gd,Lu)AlO_4 crystal with 10.8 at.% Lu^{3+} (composition #2) measured under excitation to the $^3H_4$ Tm^{3+} multiplet are shown in Fig. 2 and compared with those for a similar crystal grown without addition of Lu^{3+}. The spectra show a clear polarization-anisotropy (higher luminescence intensity is observed for π-polarization). The observed luminescence is due to the $^3F_4 \rightarrow {}^3H_6$ Tm^{3+} transition (local peaks at ~1.71, 1.76 and 1.81 μm) and the $^5I_7 \rightarrow {}^5I_8$ Ho^{3+} transition (local peaks at ~1.92, 1.96, 1.98, 2.0 and 2.08 μm). The Ho^{3+} emission dominates in the spectrum despite the much lower Ho^{3+} doping concentration. For the crystal with 10.8 at.% Lu^{3+}, the emission bandwidth $\Delta\lambda_{lum}$ (evaluating only the Ho^{3+} luminescence) is 84 nm (π-polarization) and 145 nm (σ-polarization). As compared to the crystal without Lu^{3+}, a clear spectral broadening is observed for the latter polarization (for Tm,Ho:$CaGdAlO_4$, $\Delta\lambda_{lum} = 123$ nm) and the Ho^{3+} emission spectrum experiences a red-shift of ~10 nm. For π-polarization, the effect of Lu^{3+} cooping on the luminescence spectrum is less clear.

3.2. $Tm^{3+} \leftrightarrow Ho^{3+}$ energy transfer

The parameters of the bidirectional $Tm^{3+} \leftrightarrow Ho^{3+}$ ET in the Ca(Gd,Lu)AlO_4 crystal were quantified using the dynamical model developed by Walsh et al. [9,28]. The crystal with 10.8 at.% Lu^{3+} (composition #2) was studied. The excitation was directly to the $^3F_4$ state of Tm^{3+} (at 1.70 μm) and the luminescence was monitored at two wavelengths corresponding to nearly pure Tm^{3+} (at 1.80 μm) and Ho^{3+} (at 2.04 μm) emission, cf. Fig. 2.

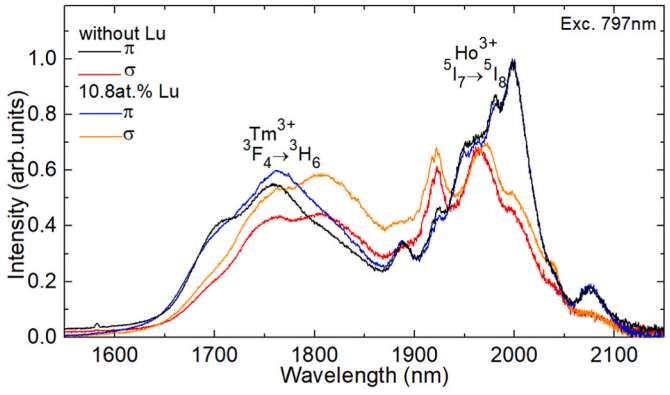

Fig. 2. Polarized luminescence spectra at ~2 μm of the Tm,Ho:Ca(Gd,Lu)AlO_4 crystal with 10.8 at.% Lu^{3+}; the spectra for a Tm,Ho:$CaGdAlO_4$ crystal are given for comparison. The light polarizations are π and σ. $\lambda_{exc} = 797$ nm.

The obtained luminescence decay curves are shown in Fig. 3. In Fig. 3(a), a close look at the very beginning of the decay is presented. The decay curves for both Tm^{3+} and Ho^{3+} ions are clearly non single exponential, and they are different from each other. Initially, a fast rise of Ho^{3+} luminescence (within few hundreds of μs) is accompanied by a respective fast reduction of luminescence intensity for Tm^{3+} ions. It represents the direct $Tm^{3+} \rightarrow Ho^{3+}$ energy transfer before the thermal equilibrium has set in. At longer times, the luminescence from the $^3F_4$ Tm^{3+} and $^5I_7$ Ho^{3+} manifolds decays with nearly the same rate. During this stage of decay, the bidirectional energy transfer takes place, but it is hidden by thermal quasi-equilibrium between the involved multiplets.

The luminescence decay curves were fitted using the following model [9]:

$$\frac{n_2(t)}{n_2(0)} = \frac{\beta}{\alpha+\beta}\exp(-t/\tau) + \frac{\alpha}{\alpha+\beta}\exp(-(\alpha+\beta)t), \quad (1a)$$

$$\frac{n_7(t)}{n_7(0)} = \frac{\alpha}{\alpha+\beta}\exp(-t/\tau) - \frac{\alpha}{\alpha+\beta}\exp(-(\alpha+\beta)t). \quad (1b)$$

Here, t is time after a short-pulse excitation, τ is the thermal equilibrium decay time, n_2 and n_7 are the electronic populations of the $^3F_4$ Tm^{3+} and $^5I_7$ Ho^{3+} states, $\alpha = P_{28}N_{Ho}$ and $\beta = P_{71}N_{Tm}$ are the transfer rates, where P_{28} is a parameter describing a direct nonradiative transfer of energy from an excited Tm^{3+} ion to a Ho^{3+} ion in the ground-state ($^5I_8$) and P_{71} is the parameter describing back nonradiative transfer of energy from an excited Ho^{3+} ion to a Tm^{3+} in the ground-state ($^3H_6$), N_{Tm} and N_{Ho} are the actual Tm^{3+} and Ho^{3+} ion densities, respectively. The fitted decay curves are shown in Fig. 3(a). The corresponding best-fit parameters are $P_{28} = 1.42 \pm 0.05$ and $P_{71} = 0.090 \pm 0.004$ [10^{-22}

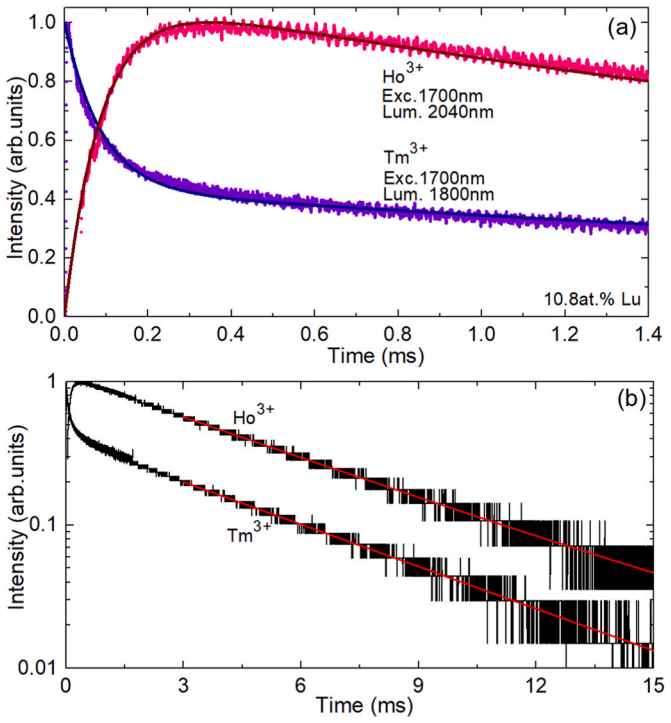

Fig. 3. (a,b) Luminescence decay curves for Tm^{3+} ions (the $^3F_4 \rightarrow {}^3H_6$ transition, $\lambda_{lum} = 1800$ nm) and Ho^{3+} ions (the $^5I_7 \rightarrow {}^5I_8$ transition, $\lambda_{lum} = 2040$ nm) in Ca(Gd,Lu)AlO_4 crystal with 10.8 at.% Lu^{3+}, (a) beginning of the decay, *symbols* – experimental data, *curves* – their fitting using Eq. (1), (b) full time scale, *lines* – single-exponential fits. $\lambda_{exc} = 1700$ nm.

$cm^3 \mu s^{-1}$] and $\tau = 4.35 \pm 0.1$ ms.

The obtained thermal equilibrium decay time for a Tm^{3+},Ho^{3+}-codoped Ca(Gd,Lu)AlO_4 crystal takes an intermediate place between the luminescence decay times for a singly Tm^{3+}-doped $CaGdAlO_4$ crystal ($\tau_{lum} = 3.20$ ms [24]) and a singly Ho^{3+}-doped one ($\tau_{lum} = 8.64$ ms [29], a value expected to be overestimated due to the radiation trapping effect in bulk samples). In the previous work [15], the luminescence decay for a Tm,Ho:$CaGdAlO_4$ crystal was studied without separating the Tm^{3+} and Ho^{3+} emissions yielding a mean decay time of 5.23 ms. This value is probably overestimated as well due to the same reason as explained above.

The ratio of energy transfer parameters, $\Theta = P_{71}/P_{28}$, is referred as an equilibrium constant. For Tm,Ho:Ca(Gd,Lu)AlO_4, $\Theta = 0.064 \pm 0.006$. The equilibrium constant allows one to evaluate the way the Tm^{3+} and Ho^{3+} ions are sharing the excitation energy. The determined small value of Θ manifests a strong prevalence of direct $Tm^{3+} \rightarrow Ho^{3+}$ energy transfer which indicates a low probability of Tm^{3+} and Ho^{3+} colasing [30] which is an unwanted effect for Tm^{3+},Ho^{3+}-codoped gain media. The determined Θ value is even smaller than those for the Tm,Ho:$KY(WO_4)_2$ ($\Theta = 0.069$) [31] and Tm,Ho:$LiYF_4$ ($\Theta = 0.076$) [9] crystals.

The equilibrium constant Θ (concentration-independent) for a Tm^{3+}, Ho^{3+}-codoped crystal is estimated from the crystal-field splitting of the multiplets of Tm^{3+} and Ho^{3+} ions involved in the energy-transfer [9]:

$$\Theta = \frac{Z_2 Z_8}{Z_1 Z_7} \exp\left[-\left(E_{ZPL}^{Tm} - E_{ZPL}^{Ho}\right)/kT\right], \quad (2)$$

where Z_1, Z_2, Z_7 and Z_8 are the partition functions of the $^3H_6$ Tm^{3+}, $^3F_4$ Tm^{3+}, $^5I_7$ Ho^{3+} and $^5I_8$ Ho^{3+} multiplets, respectively, E_{ZPL} are the energies of the zero-phonon-line (ZPL) transitions occurring between the lowest Stark levels of the ground and excited manifolds (this work, see below), k is the Boltzmann constant and T is the crystal temperature (RT). Due to the availability of the crystal-field data for Tm^{3+} and Ho^{3+} ions in the isostructural $CaYAlO_4$ crystal [32], they were used for calculation of the partition functions yielding $\Theta = 0.056$ that is close to the experimental value.

3.3. Low-temperature spectroscopy

The inhomogeneous broadening of the spectral bands of Tm^{3+} and Ho^{3+} ions in the Ca(Gd,Lu)AlO_4 crystal is revealed at low temperature. The LT absorption studies were used to determine the experimental crystal-field splitting of excited-states of Tm^{3+} (from $^3F_4$ to $^1D_2$) and Ho^{3+} (from $^5I_7$ to $^5F_5$). In particular, the absorption bands corresponding to the $^3H_6 \rightarrow {}^3F_4$, $^3H_5$ and $^3H_4$ Tm^{3+} and $^5I_8 \rightarrow {}^5I_7$ and $^5I_6$ Ho^{3+} transitions are shown in Fig. 4 for π- and σ-polarized light. The horizontal axis in this figure is plotted in wavenumbers ($\nu = 1/\lambda$, in cm^{-1}) to facilitate the assignment of electronic transitions. The LT luminescence studies were also performed to conclude about the experimental crystal-field splitting of the ground-states of Tm^{3+} ($^3H_6$) and Ho^{3+} ($^5I_8$). Fig. 5 shows the emission bands corresponding to the $^5I_7 \rightarrow {}^5I_8$ Ho^{3+}, $^3F_4 \rightarrow {}^3H_6$, $^3H_4 \rightarrow {}^3H_6$ and $^3H_4 \rightarrow {}^3F_4$ Tm^{3+} transitions. In this figure, the horizontal axis is plotted in (E_{ZPL} – wavenumber, in cm^{-1}) to directly access the energies of Stark sub-levels of the terminal levels. The spectra remain smooth and broad even at 12 K.

Hutchinson et al. calculated the positions of the energy levels of Tm^{3+} and Ho^{3+} ions in the isostructural $CaYAlO_4$ crystal using a quantum mechanical point charge model [32]. The authors used S_4 symmetry as an approximation to the C_{4v} one (the local symmetry of the rare-earth site in $CaLnAlO_4$ crystals according to the structure refinement data, see Ref. [25]). For the S_4 symmetry, the total number of Stark sub-levels for a $^{2S+1}L_J$ multiplet with an even J is less than 2 J + 1, i.e., it is 13, 11, 10, 8, 7, 5, 4 and 2 and 7 for J = 8, 7, 6, 5, 4, 3, 2 and 1, respectively. Following the data on the crystal-field splitting from Ref. [32], we made an attempt to determine the experimental positions of the Stark sub-levels of excited multiplets of Tm^{3+} and Ho^{3+} ions in the Ca(Gd,Lu)

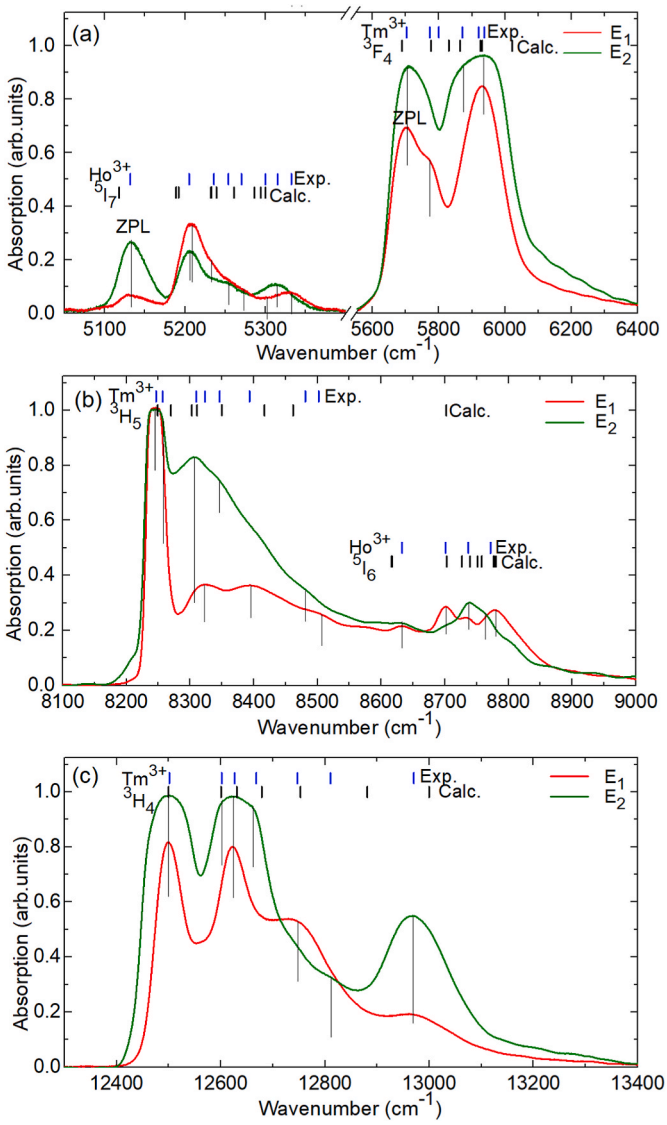

Fig. 4. LT (12 K) absorption spectra of Tm^{3+} and Ho^{3+} ions in the Ca(Gd,Lu)AlO_4 crystal with 10.8 at.% Lu^{3+}: (a) the $^3H_6 \rightarrow {}^3F_4$ Tm^{3+} and $^5I_8 \rightarrow {}^5I_7$ Ho^{3+} transitions; (b) the $^3H_6 \rightarrow {}^3H_5$ Tm^{3+} and $^5I_8 \rightarrow {}^5I_6$ Ho^{3+} transitions; (c) the $^3H_6 \rightarrow {}^3H_4$ Tm^{3+} transition, *black dashes* – theoretical crystal-field splitting for $CaYAlO_4$ from Ref. [32], *blue dashes* – experimental energies of Stark sub-levels. $\boldsymbol{E}_1$ and $\boldsymbol{E}_2$ are the light polarizations (σ and π, respectively). ZPL – positions of the zero-phonon lines for laser transitions.

AlO_4 crystal, cf. Table 1. The introduction of Lu^{3+} is expected to modify the composition of the second coordination sphere around the active ions (the multi-ligands) leading to additional inhomogeneous spectral broadening and could distort the site symmetry. However, according to the structural [25] and spectroscopic (this work) studies of the Tm,Ho:Ca(Gd,Lu)AlO_4 crystals, the presence of up to 10.8 at.% Lu^{3+} does not reduce the local site symmetry.

Fig. 6 summarizes the obtained data on the experimental energy levels of Tm^{3+} and Ho^{3+} ions in the Ca(Gd,Lu)AlO_4 crystal. In the same figure, we also describe the spectroscopic processes relevant for achieving Ho laser emission at ~2 μm. After excitation at ~0.8 μm (to the $^3H_4$ Tm^{3+} state), the Tm^{3+} ions can experience a two-step multi-phonon non-radiative relaxation to the lower-lying metastable $^3F_4$ state (the most intense Raman mode of Ca(Gd,Lu)AlO_4 is at 311 cm^{-1} and the maximum phonon energy is ~650 cm^{-1}, cf. Ref. [25]). Alternatively, it can be populated via the cross-relaxation process which is promoted by high Tm^{3+} doping concentration, $^3H_4 + {}^3H_6 \rightarrow {}^3F_4 + {}^3F_4$. As the

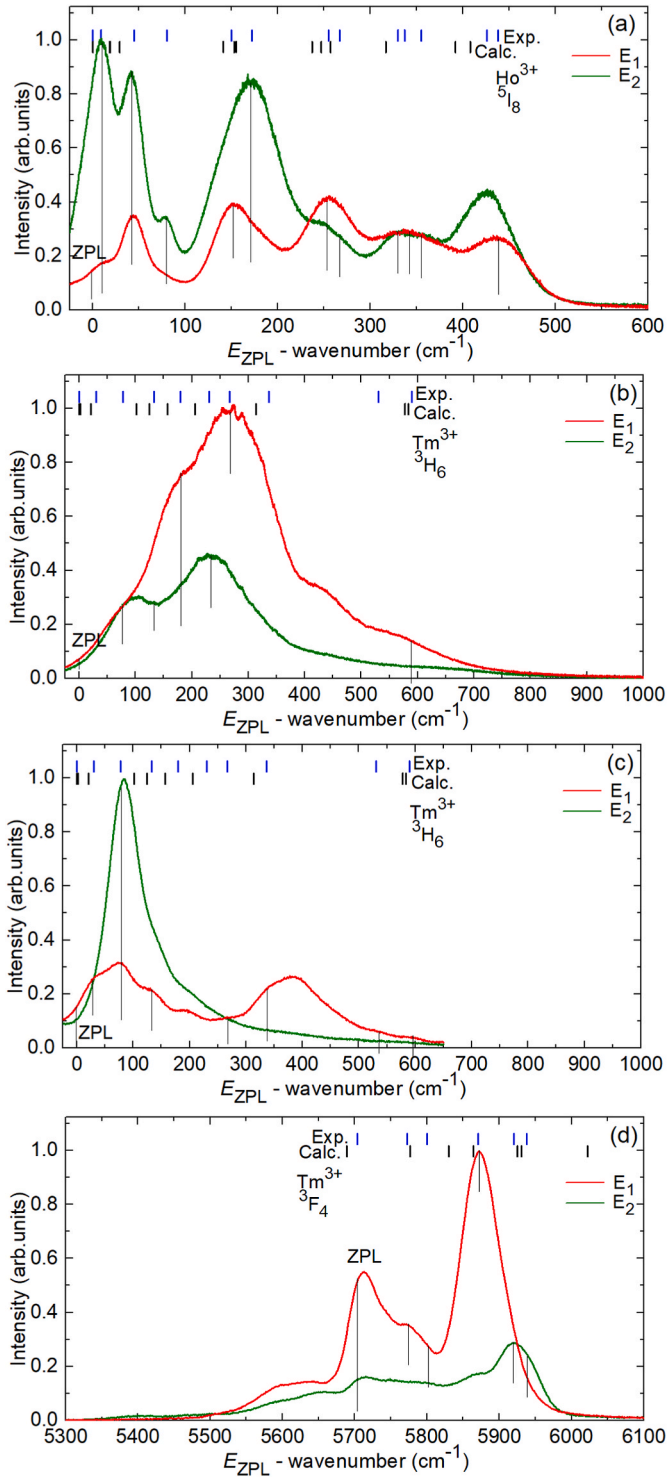

Fig. 5. LT luminescence spectra of Tm^{3+} and Ho^{3+} ions in the Ca(Gd,Lu)AlO_4 crystal with 10.8 at.% Lu^{3+}: (a) the $^5I_7 \rightarrow {}^5I_8$ Ho^{3+} transition; (b) the $^3F_4 \rightarrow {}^3H_6$ Tm^{3+} transition; (c) the $^3H_4 \rightarrow {}^3H_6$ Tm^{3+} transition; (d) the $^3H_4 \rightarrow {}^3F_4$ Tm^{3+} transition, *black dashes* – theoretical crystal-field splitting for $CaYAlO_4$ from Ref. [32], *blue dashes* – experimental energies of Stark sub-levels. $\boldsymbol{E}_1$ and $\boldsymbol{E}_2$ are the light polarizations (σ and π, respectively). ZPL – positions of the zero-phonon lines for laser transitions.

Table 1
Experimental crystal-field splitting for Tm^{3+} and Ho^{3+} ions in the Ca(Gd,Lu)AlO_4 crystal. The total number of sub-levels correspond to the S_4 symmetry. *L – luminescence spectra, A – absorption spectra.

$^{2S+1}L_J$	Data*	Energy, cm^{-1}
		Tm^{3+} ions
$^3H_6$	L	0; 30; 78; 133; 180; 231; 267; 337; 531; 590
$^3F_4$	A, L	5703; 5773; 5800; 5871; 5920; 5938 *(1 missing)*
$^3H_5$	A	8246; 8257; 8309; 8323; 8346; 8393; 8481; 8502 (?)
$^3H_4$	A	12,501; 12,602; 12,626; 12,668; 12,747; 12,810; 12,970
$^3F_3$	A	14,442; 14,571 *(3 missing)*
$^3F_2$	A	14,967; 15,013; 15,158 *(1 missing)*
$^1G_4$	A	21,148; 21,303; 21,366; 21,407; 21,482 *(2 missing)*
$^1D_2$	A	27,643; 27,744; 27,919 *(1 missing)*
		Ho^{3+} ions
$^5I_8$	L	0; 9; 45; 80; 150; 172; 255; 267; 330; 337; 355; 426; 438
$^5I_7$	A	5132; 5205; 5236; 5254; 5270; 5300; 5315; 5332 *(3 missing)*
$^5I_6$	A	8632; 8700; 8736; 8771 *(6 missing)*
$^5I_5$	A	11,283; 11,304; 11,338 *(5 missing)*
$^5I_4$	A	13,186; 13,268; 13,310; 13,445 *(3 missing)*
$^5F_5$	A	15,427; 15,458; 15,523; 15,588 *(4 missing)*
$^5S_2$	A	18,454; 18,484; 18,529 (?) *(1 missing)*
$^5F_4$	A	18,570 (?); 18,681 *(5 missing)*
$^5F_3$	A	20,544; 20,588; 20,662; 20,681 *(1 missing)*
$^5G_6$	A	22,002; 22,046; 22,100; 22,199; 22,348 *(5 missing)*
$^5F_1$	A	22,527 *(1 missing)*
$^3G_5$	A	23,872; 23,960; 24,027 *(5 missing)*
$^5G_4$	A	25,843; 25,933 *(5 missing)*
$^5F_5$	A	26,155; 26,213 *(6 missing)*

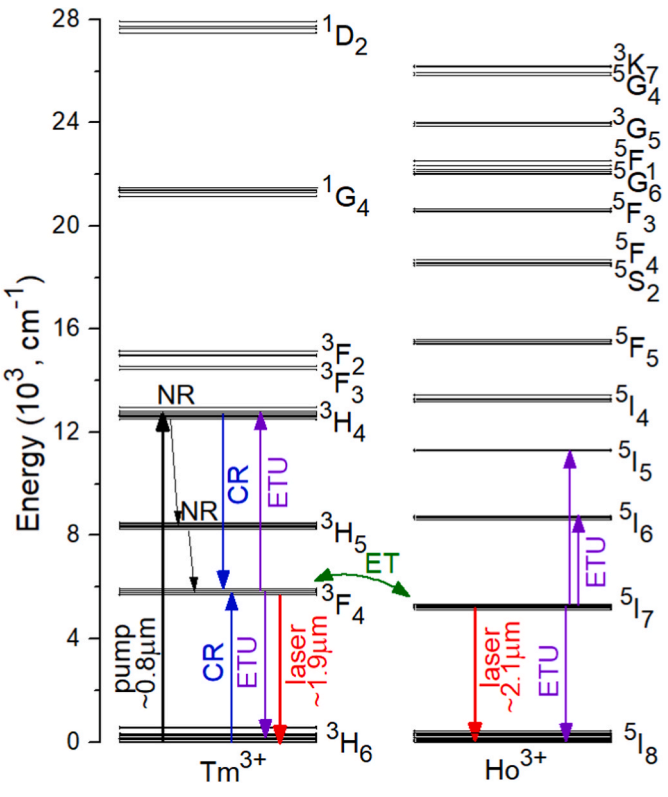

Fig. 6. Scheme of energy-level of Tm^{3+} and Ho^{3+} ions in the Ca(Gd,Lu)AlO_4 crystal: black and red arrows – pump and laser transitions, respectively, CR - cross-relaxation, ETU – energy-transfer upconversion, ET – energy-transfer, NR – multi-phonon non-radiative relaxation.

barycenter of the $^3F_4$ Tm^{3+} multiplet is positioned slightly higher in energy than that of the $^5I_7$ Ho^{3+} multiplet, predominantly unidirectional $Tm^{3+} \rightarrow Ho^{3+}$ ET occurs (expressed by the determined equilibrium constant Θ) followed by laser emission according to the $^5I_7 \rightarrow {}^5I_8$ Ho^{3+} transition. Due to the overlap of the gain spectra of Tm^{3+} and Ho^{3+} ions (see below), when using a spectrally selective intracavity element, $^3F_4 \rightarrow {}^3H_6$ Tm^{3+} laser emission can be also forced.

3.4. Stimulated-emission and gain cross-sections

At first, we have determined the absorption, σ_{abs}, and stimulated-emission (SE), σ_{SE}, cross-sections for the $^3F_4 \leftrightarrow {}^3H_6$ Tm^{3+} and $^5I_7 \leftrightarrow {}^5I_8$ Ho^{3+} transitions in the Ca(Gd,Lu)AlO_4 crystal, as shown in Fig. 7 for light polarizations π and σ.

The absorption of the Ho^{3+} ions was obtained by subtracting the Tm^{3+} contribution from the spectra of the codoped crystal and using the formula $\sigma_{abs} = \alpha_{abs}/N_{Ho}$. For the $^5I_8 \rightarrow {}^5I_7$ Ho^{3+} transition in absorption, the peak σ_{abs} is 0.66×10^{-20} cm^2 at 1921 nm (σ-polarization) and 0.63×10^{-20} cm^2 at 1948 nm (π-polarization). The Tm^{3+} absorption was quantified using a singly doped crystal [24]. For the $^3H_6 \rightarrow {}^3F_4$ Tm^{3+} transition in absorption, the anisotropy of absorption cross-sections is much higher, namely, the peak σ_{abs} is 0.65×10^{-20} cm^2 at 1736 nm (σ-polarization) and 1.15×10^{-20} cm^2 at 1698 nm (π-polarization).

The SE cross-section spectra for both ions were determined using a combination of the Füchtbauer–Ladenburg (F-L) equation [33] and the reciprocity method (RM) [34]. In the former case, the following radiative lifetimes of the upper manifolds were used: for the $^3F_4$ state of Tm^{3+}, $\tau_{rad} = 2.46$ ms (determined by the J-O theory [24]) and for the $^5I_7$ state of Ho^{3+}, $\tau_{rad} = 3.32$ ms (obtained by the same approach, see Ref. [25]). The refractive indices of $CaGdAlO_4$ were taken from Ref. [27], i.e., $n_o = 1.901$ and $n_e = 1.924$ at ~2 μm.

For the RM, the partition functions Z_m for both, the lower ($m = 1$) and upper ($m = 2$) manifolds, were calculated using the crystal-field splitting from Hutchinson et al. [32] for the isostructural $CaYAlO_4$ crystal. The obtained values are $Z_1(^3H_6) = 6.945$, $Z_2(^3F_4) = 4.345$, so that $Z_1/Z_2 = 1.599$ (for Tm^{3+} ions) and $Z_1(^5I_8) = 8.315$, $Z_2(^5I_7) = 8.966$, so that $Z_1/Z_2 = 0.927$ (for Ho^{3+} ions). The energies of the ZPL transitions were taken from the data from LT spectroscopy, cf. Tables 1 and i.e., $E_{ZPL} = 5703$ cm^{-1} for Tm^{3+} and 5133 cm^{-1} for Ho^{3+}. The σ_{SE} obtained by the two methods were in good agreement with each other.

For the $^5I_7 \rightarrow {}^5I_8$ Ho^{3+} transition in emission, the maximum SE cross-section is $\sigma_{SE} = 0.50 \times 10^{-20}$ cm^2 at 1973 nm (σ-polarization) and 1.05×10^{-20} cm^2 at 2000 nm (π-polarization). The observed strong polarization anisotropy of SE cross-sections manifests the possibility for linearly polarized laser emission for ***a***-cut crystals. Note that Ho^{3+} lasers represent a quasi-three-level scheme with reabsorption. Consequently, the laser generation is expected to occur at wavelengths longer than the ZPL position. The inspection of the σ_{SE} spectra reveals a very intense local peak at ~2.08 μm corresponding to even stronger polarization-anisotropy of the emission properties: $\sigma_{SE} = 0.20 \times 10^{-20}$ cm^2 (σ-polarization) and 0.71×10^{-20} cm^2 (π-polarization).

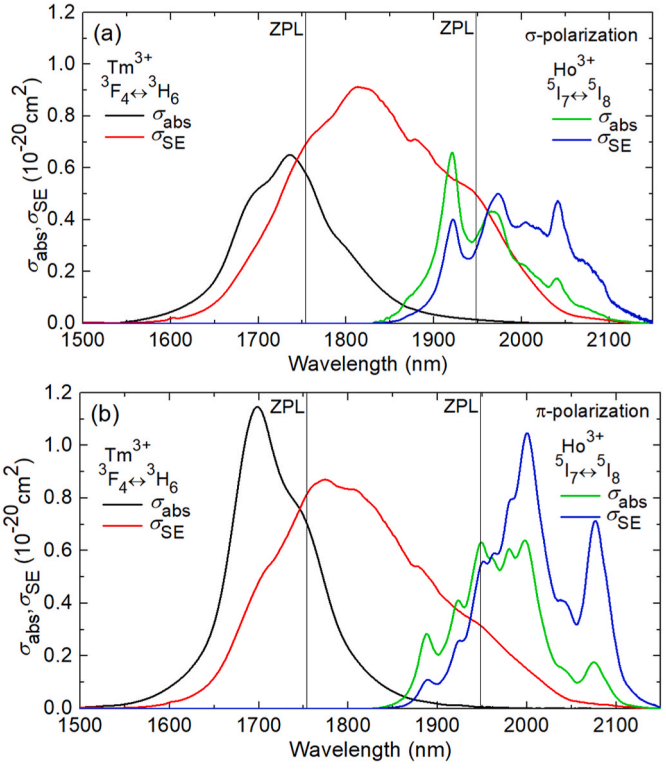

Fig. 7. Absorption, σ_{abs}, and stimulated-emission (SE), σ_{SE}, cross-sections for the $^3F_4 \leftrightarrow {}^3H_6$ Tm^{3+} and $^5I_7 \leftrightarrow {}^5I_8$ Ho^{3+} transitions for the Tm,Ho:Ca(Gd,Lu)AlO_4 crystal, the light polarization is (a) σ and (b) π.

For quasi-three-level laser transitions, it is common to calculate the gain cross-section spectra accounting for different reabsorption under particular inversion levels in the gain medium. The gain spectra are useful to predict the laser wavelength in free-running lasers and its change with the output coupling, to conclude about the possible wavelength tuning range and to estimate the gain bandwidth which is relevant for ML lasers.

When treating the Tm^{3+} and Ho^{3+} ions separately, the gain cross-sections are:

$$\sigma_{g,Tm(Ho)} = \beta_{Tm(Ho)}\sigma_{SE,Tm(Ho)} - \left(1 - \beta_{Tm(Ho)}\right)\sigma_{abs,Tm(Ho)}, \tag{3}$$

where, $\beta_{Tm} = N_2(^3F_4)/N_{Tm}$ and $\beta_{Ho} = N_7(^5I_7)/N_{Ho}$ are the inversion levels for both, Tm^{3+} and Ho^{3+} ions, respectively, and N_2 and N_7 are the populations of the $^3F_4$ Tm^{3+} and $^5I_7$ Ho^{3+} upper laser levels, respectively (we follow the notations for the populations proposed by Walsh et al. [9]).

In the case of a Tm^{3+},Ho^{3+}-codoped material, one cannot treat the $\sigma_{g,Tm}$ and $\sigma_{g,Ho}$ spectra separately. In the thermal equilibrium regime, the populations of the excited-states of Tm^{3+} and Ho^{3+} ions are linked to each other owing to the bidirectional ET. The effective gain cross-section is then [35]:

$$\sigma_{g,eff} = \left(\beta_{Ho}\sigma_{SE,Ho} - (1 - \beta_{Ho})\sigma_{abs,Ho}\right)\frac{N_{Ho}}{N_{tot}} + \left(\beta_{Tm}\sigma_{SE,Tm} - (1 - \beta_{Tm})\sigma_{abs,Tm}\right)\frac{N_{Tm}}{N_{tot}}. \tag{4}$$

This formula accounts for both the absorption and stimulated-emission of both the Tm^{3+} and Ho^{3+} ions. The effective gain cross-section is defined with respect to the total (Tm^{3+} + Ho^{3+}) doping concentration, $N_{tot} = N_{Tm} + N_{Ho}$. From the condition of the thermal equilibrium state established by the bidirectional $Tm^{3+} \leftrightarrow Ho^{3+}$ ET, the inversion ratio for Ho^{3+} ions β_{Ho} can de derived from that for Tm^{3+} ions, β_{Tm} [35]:

$$\beta_{Ho} = \frac{\Omega\beta_{Tm}}{1 + (\Omega - 1)\beta_{Tm}}. \tag{5}$$

Here, $\Omega = 1/\Theta$ where Θ is the equilibrium constant described above.

The results on the effective gain cross-section spectra for a 4.5 at.% Tm, 0.38 at.% Ho:Ca(Gd,Lu)AlO_4 crystal are presented in Fig. 8(a,c) for light polarizations π and σ. The spectra were calculated for different Tm^{3+} inversion ratios β_{Tm} ranging between 0.015 and 0.06. The corresponding Ho^{3+} inversion ratios β_{Ho} were determined using Eq. (5).

The gain spectra for both polarizations are smooth and broad. For the same level of inversion (both β_{Tm} and β_{Ho}) set by the total cavity losses (passive and output-coupling), the gain cross-sections are higher for π-polarization. Thus, this polarization state is expected to be naturally selected in lasers based on ***a***-cut crystals. The gain spectrum for π-polarization exhibits a local maximum at ~2.08 μm and the corresponding gain bandwidth (FWHM) $\Delta\lambda_g$ is 33 nm. For σ-polarization, although the absolute values of effective gain cross-sections are lower, the gain spectra are much broader. For very small inversion ratios $\beta_{Tm} < 0.015$, the gain spectrum is centered at ~2.10 μm. With increasing β_{Tm}, it experiences a blue-shift with the local maxima first at ~2.08 μm and then at ~2.04 μm. The corresponding gain bandwidth calculated for example $\beta_{Tm} = 0.025$ and 0.035 are as broad as 66 nm and 94 nm, respectively.

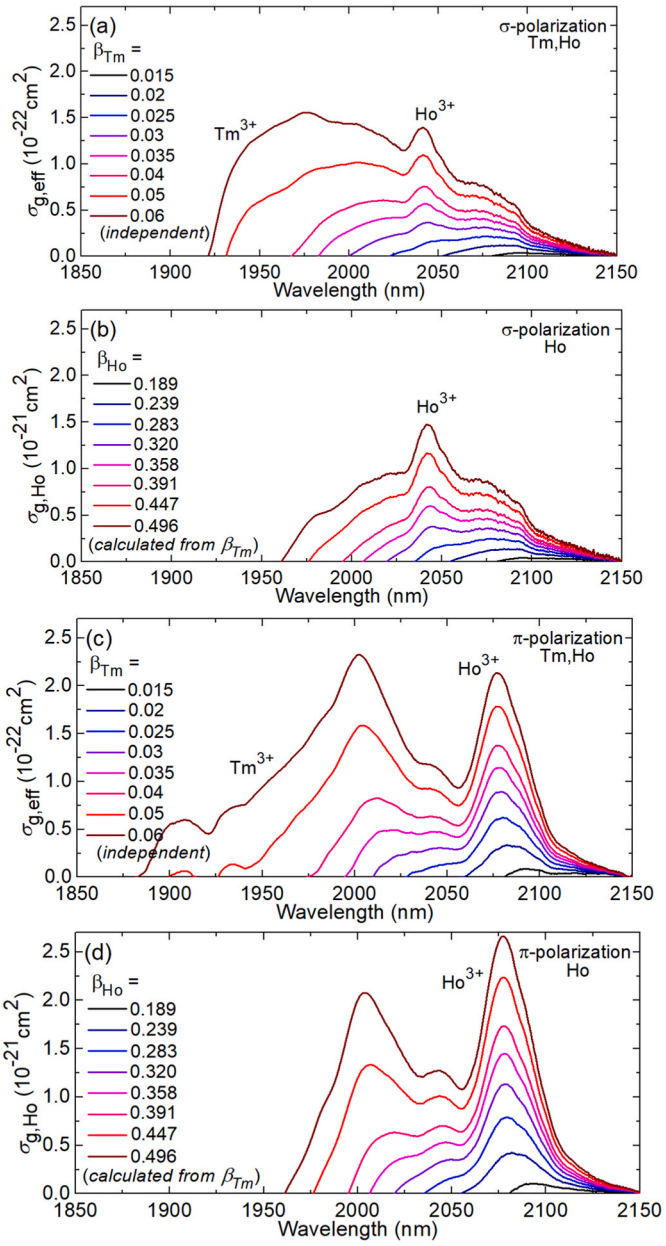

Fig. 8. (a,c) Effective gain cross-sections, $\sigma_{g,eff}$, at ~2 μm for the 4.5 at.% Tm, 0.38 at.% Ho:Ca(Gd,Lu)AlO_4 crystal with 10.8 at.% Lu^{3+}, calculated using Eq. (4), $\beta_{Tm} = N\,(^3F_4)/N_{Tm}$ is the inversion ratio for Tm^{3+} ions (independent parameter); (b,d) gain cross-sections for Ho^{3+} ions at ~2 μm, $\sigma_{g,Ho}$, for the inversion ratios for Ho^{3+} ions $\beta_{Ho} = N\,(^5I_7)/N_{Ho}$ corresponding to β_{Tm} values specified in (a,c) and calculated using Eq. (5). The light polarization is (a,b) σ and (c,d) π.

Thus, the σ-polarization is much more attractive for the generation of ultrashort pulses in ML lasers. Note that particularly for this polarization, the effect of Lu^{3+} codoping on the broadening of the luminescence spectra and their extension well beyond 2 μm is more pronounced.

To conclude about the contribution of both rare-earth ions to the gain spectra, we have calculated the gain cross-section spectra considering only the Ho^{3+} ions using Eq. (3), see Fig. 8(b,d). Here, the β_{Ho} values in the range of 0.189–0.496 corresponding to the β_{Tm} ones listed in Fig. 8(a,c) and obtained via Eq. (5) are used. The Tm^{3+} contribution becomes evident for the wavelength below 2 μm. It is also relevant for achieving broadband tuning of laser emission between ~1.9 and 2.1 μm.

4. Tunable laser operation

4.1. Laser set-up

The scheme of the X-folded laser cavity is shown in Fig. 9. It was formed by two plano-concave (radius of curvature, RoC = −100 mm) folding mirrors (M_1 and M_2) coated for high reflectance (HR) at the laser wavelength and high transmission (HT) at ~0.79 μm, a flat HR end mirror (M_3) and a set of plane-wedged output couplers (OCs) having a transmission T_{OC} of 0.2%, 0.5%, 1.5%, and 3% at the laser wavelength. The rectangular laser element prepared from the Tm,Ho:Ca(Gd,Lu)AlO_4 crystal with a Lu^{3+} content of 5.5 at.% was cut for light propagation along the ***a***-axis (***a***-cut) and it had a thickness of 6.0 mm and an aperture of 3.0 × 3.0 mm^2. Both its end-facets were polished to laser-grade quality and antireflection (AR) coated for both the pump and laser wavelengths. The crystal was wrapped with indium foil and mounted in a copper holder (temperature set at 12.0 °C by water cooling) to mitigate the thermal load. The laser element was placed between the folding mirrors. As pump source, a CW Ti:Sapphire laser delivering up to 3.5 W at 793 nm in a single-transverse mode ($M^2 \approx 1$) was used with linear polarization (corresponding to π in the crystal). An AR coated lens (f = 70 mm) was used to focus the pump beam into the crystal resulting in a waist of 60 μm (measured for normal incidence). The pumping was in single-pass.

The wavelength tuning was studied by inserting a Lyot filter (3.2 mm thick quartz plate with the optical axis at 60° to the surface) at the Brewster angle in the cavity arm formed by the folding mirror M_1 and the OC.

4.2. Free-running and tunable laser operation

First, the laser performance was studied in the free-running regime (without the Lyot filter in the cavity). The Tm, Ho laser generated a maximum output power of 763 mW at 2078.6 nm with a slope efficiency η of 26.4% (vs. the absorbed pump power) and a laser threshold P_{th} of 128 mW (using the output coupler with 3% transmission), Fig. 10(a). The measured pump absorption under lasing conditions is shown in Fig. 10(b). With increasing the incident pump power, it followed nearly the same trend for all the studied OCs, e.g., for T_{OC} = 3%, it decreased from 96.3% to 92.8% representing the effect of the ground-state bleaching. With increasing the output coupling from 0.2% to 3%, the emission wavelength experienced a blue-shift, from 2085.1 nm to 2078.6 nm, Fig. 10(c). The laser emission was linearly polarized (π).

The tuning experiment was performed using the smallest available T_{OC} = 0.2%. The laser polarization was set to σ by the orientation of the Lyot filter. The pump laser was tuned to 801.3 nm and the absorbed pump power P_{abs} amounted to 3.14 W. A continuous tuning of laser emission between 1887.7 and 2127 nm (i.e., a tuning range of 239.3 nm) was achieved, Fig. 11. The maximum output power of 312 nm was achieved at 2114 nm.

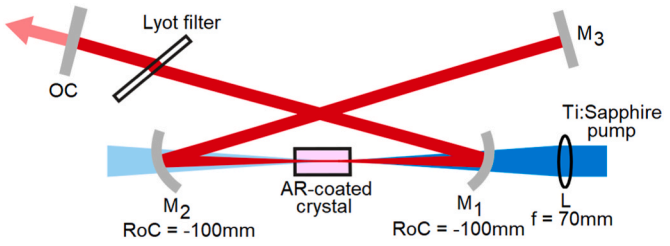

Fig. 9. Scheme of the tunable Tm,Ho:Ca(Gd,Lu)AlO_4 laser: L - focusing lens (f – focal length), M1 and M2 – folding mirrors (RoC – radius of curvature), M3 – HR mirror, OC – output coupler.

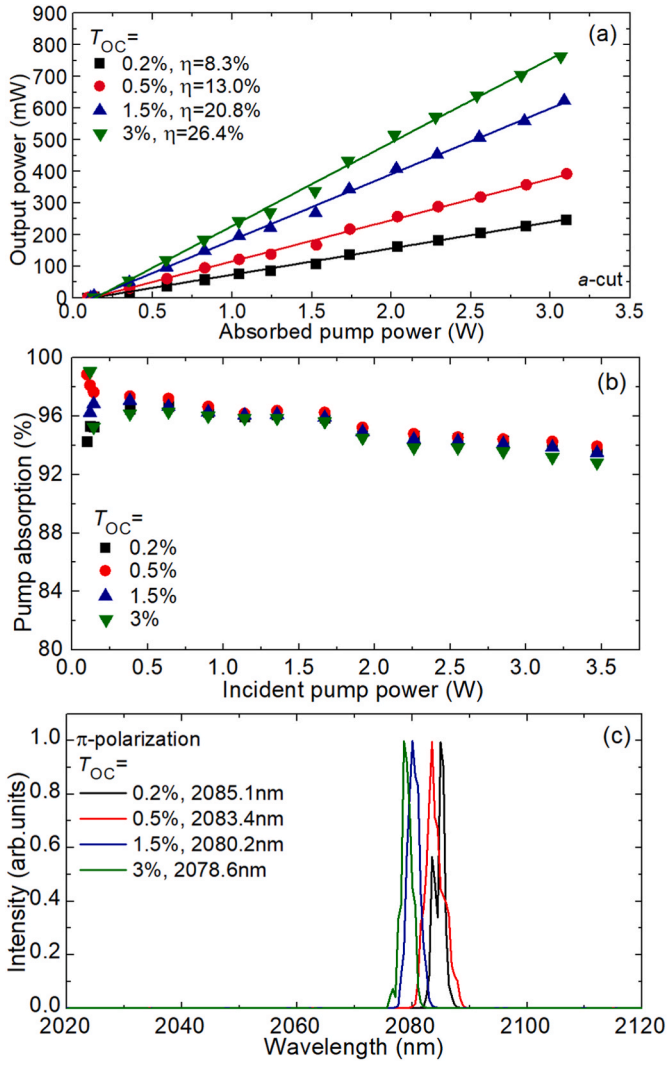

Fig. 10. Ti:Sapphire pumped free-running Tm,Ho:Ca(Gd,Lu)AlO_4 laser: (a) input-output dependences; (b) pump absorption under lasing conditions (single pass); (c) typical spectra of laser emission, ***a***-cut crystal, π-polarized emission. Lu^{3+} content: 5.5 at.%.

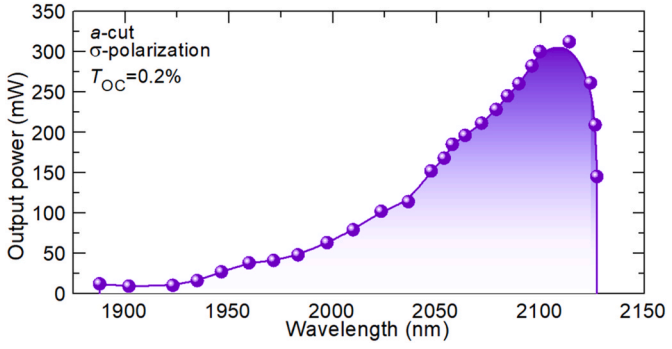

Fig. 11. Tuning curve for the Tm,Ho:Ca(Gd,Lu)AlO_4 laser: ***a***-cut crystal, σ-polarized laser emission, P_{abs} = 3.14 W, T_{OC} = 0.2%. Lu^{3+} content: 5.5 at.%.

4.3. Diode-pumped laser operation

4.3.1. Laser set-up

The diode-pumped laser performance was studied in a simple plane-plane (microchip type) laser cavity, Fig. 12. It is feasible because of the positive (focusing) thermal lens for $CaGdAlO_4$ crystals [36]. Two rectangular laser elements were cut from each of the two studied Tm,Ho:Ca(Gd,Lu)AlO_4 crystals. They were oriented for light propagation along the [100] and [001] crystallographic axes (***a***-cut and ***c***-cut, respectively). The elements had a thickness t of 3.0 mm and an aperture of 3.0 × 3.0 mm^2. Their input and output faces were polished to laser-grade quality with good parallelism and remained uncoated. The elements were wrapped into Indium foil from 4 lateral sides and mounted in a Cu-holder cooled by circulating water (12 °C). The laser cavity was formed by a flat pump mirror (PM) coated for high transmission (HT) at 0.80 μm (the pump wavelength) and for high reflection (HR) at 1.8–2.1 μm. A set of flat output couplers (OCs) was used with measured transmission T_{OC} = 0.1%, 1.5%, 3% and 5% at the laser wavelength. Both the PM and the OC were placed near the crystal surfaces with minimum air gaps leading to a geometrical cavity length of ~3 mm.

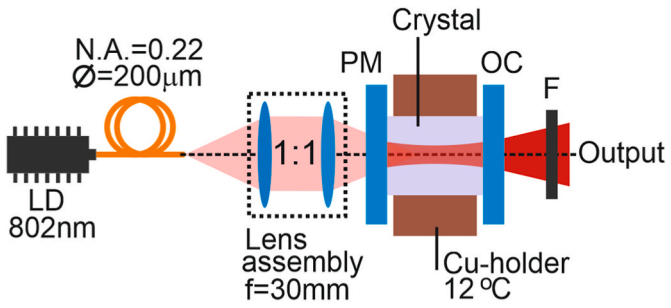

Fig. 12. Scheme of the compact diode-pumped Tm,Ho:Ca(Gd,Lu)AlO_4 laser: LD – laser diode, PM – pump mirror, OC – output coupler, F – cut-off filter.

As a pump source a fiber-coupled (core diameter: 200 μm, N.A. = 0.22) AlGaAs laser diode (LD) at ~802 nm (M^2 > 80) was used. The emission wavelength of the LD was stabilized by fixing the temperature with circulating water. The pump beam was focused into the crystal through the PM with an antireflection (AR) coated lens assembly (reimaging ratio: 1:1, focal length: f = 30 mm). The pump spot size in the focus amounted to $2w_P = 200 \pm 10$ μm with a confocal parameter $2z_R$ = 1.8 mm. Partial reflection at the pump wavelength ($R \approx 40\%$) was provided by the OCs. We calculated the total (double-pass) pump absorption by means of pump-transmission measurements under non-lasing conditions at the threshold pump power. It was weakly dependent on the output coupling. For the crystal with 5.5 at.% Lu^{3+}, η_{abs} (2-passes) was 66.2% (***a***-cut) and 65.6% (***c***-cut).

The laser emission spectra were measured using a spectrum analyzer (model WaveScan, 1000–2600 nm, APE GmbH) with a resolution of 0.2 nm.

4.4. Diode-pumped laser operation

CW laser operation was achieved with ***a***-cut and ***c***-cut Tm,Ho:Ca(Gd,Lu)AlO_4 crystals of both compositions. The input-output dependences and the typical laser spectra for the crystal with 5.5 at.% Lu^{3+} are shown in Fig. 13. Slightly better performance was achieved for the ***c***-cut laser element: the laser generated a maximum output power of 310 mW at 2085.0 nm with a slope efficiency η of 9.7% (vs. the absorbed pump power P_{abs}) and a laser threshold P_{th} of 1.21 W (for T_{OC} = 1.5%), Fig. 13 (c). The laser threshold gradually increased with the output coupling, from 1.02 W (T_{OC} = 0.1%) up to 2.29 W (T_{OC} = 5%). A thermal roll-over in the output dependences was observed for P_{abs} > 4 W. It is assigned to upconversion in the (Tm^{3+}, Ho^{3+}) system causing serious thermal issues. For the ***a***-cut laser element, the laser performance was slightly inferior, Fig. 13(a). A summary of the output characteristics of diode-pumped Tm,Ho:Ca(Gd,Lu)AlO_4 lasers is given in Table 2.

For the ***c***-cut laser elements, the laser emission was unpolarized. In the $CaGdAlO_4$ crystal, the optical axis is parallel to the ***c***-axis, so all the waves propagating along this direction correspond to *o*-waves

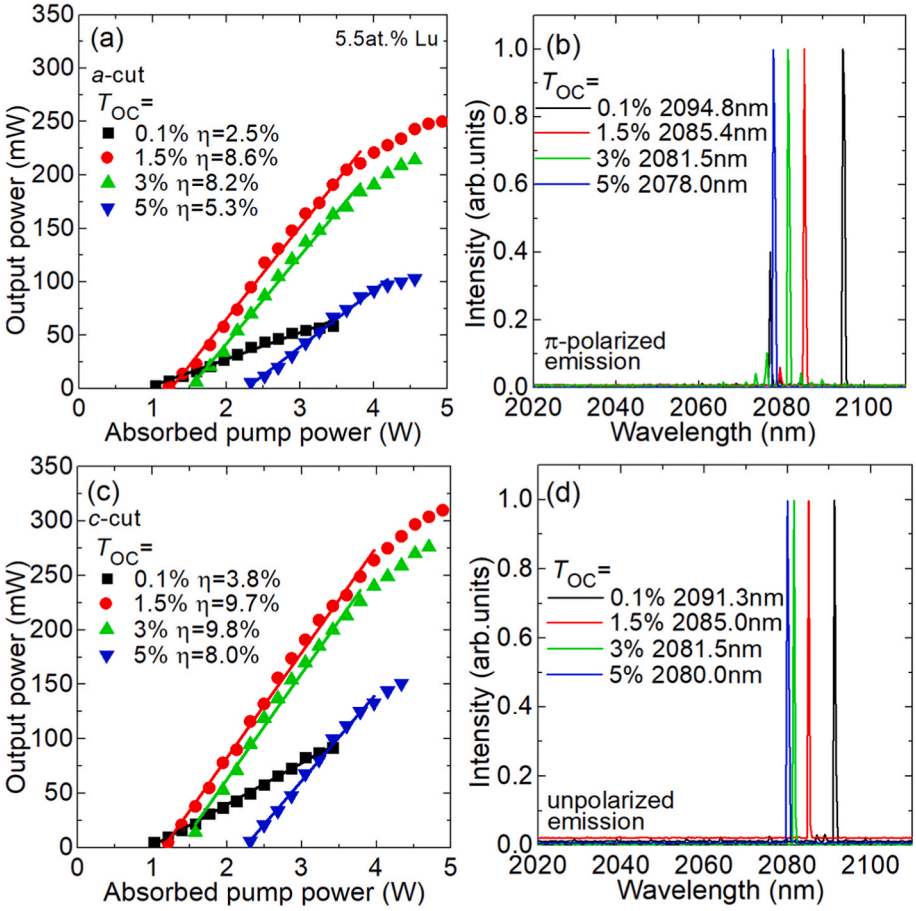

Fig. 13. Diode-pumped compact Tm,Ho:Ca(Gd,Lu)AlO_4 laser: (a,c) input-output dependences, (b,d) typical spectra of laser emission measured at maximum P_{abs}, (a, b) ***a***-cut crystal, π-polarized emission, (c,d) ***c***-cut crystal, unpolarized emission. Lu^{3+} content: 5.5 at.%.

Table 2
Output characteristics of diode-pumped Tm,Ho:Ca(Gd,Lu)AlO_4 lasers.

Sample: Lu^{3+} content	Crystal cut	P_{out}, mW	η, %	P_{th}, W	λ_L, nm	Polariz.
5.5 at.%	***a***-cut	250	8.6	1.22	2085.4	π
	c-cut	**310**	**9.7**	**1.21**	2085.0	unpolar.
10.8 at.%	***a***-cut	198	8.5	2.17	2088.9	π
	c-cut	185	4.7	2.56	2073.5	unpolar.

P_{out} – output power, η – slope efficiency, P_{th} – laser threshold, λ_L – laser wavelength. T_{OC} = 1.5%.

(σ-polarization). For the ***a***-cut elements, the emission was linearly polarized, and the polarization state (π) was naturally selected by the gain anisotropy in agreement with the gain spectra for small inversion ratios β_{Tm}, Fig. 8. The typical laser spectra are shown in Fig. 13(b,d). They are similar for ***a***-cut and ***c***-cut crystals. The emission occurred around ~2.08 μm, assigned exclusively to the $^5I_7 \rightarrow {}^5I_8$ Ho^{3+} transition. The laser wavelength experienced a slight blue-shift with the output coupling, e.g., from 2094.8 nm (T_{OC} = 0.1%) to 2078.0 nm (T_{OC} = 5%) for the ***c***-cut crystal. This shift is due to the quasi-three-level nature of the Ho^{3+} laser scheme.

The introduction of rare-earth dopants in high concentrations into the $CaGdAlO_4$ host crystal is expected to reduce its optical quality, thermal conductivity and thermal shock resistance ability. To reveal the effect of Lu^{3+} addition, we compared the output performances of diode-pumped Tm,Ho:Ca(Gd,Lu)AlO_4 lasers based on two crystals with the same cut (***a***-cut) while different Lu^{3+} content, as shown in Fig. 14. For the crystal with 10.8 at.% Lu^{3+}, the laser performance clearly

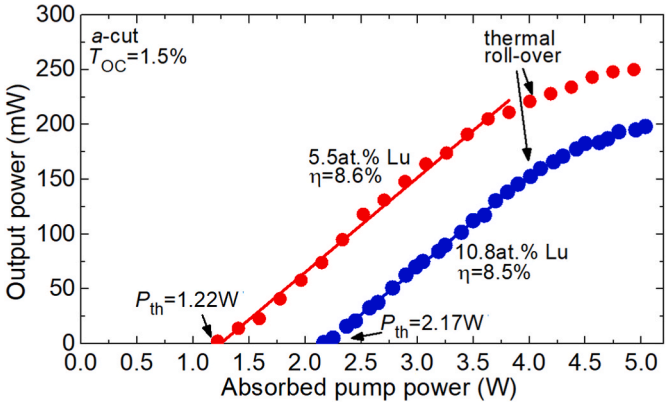

Fig. 14. Comparison of output performances of diode-pumped Tm,Ho:Ca(Gd, Lu)AlO_4 lasers based on crystals containing 5.5 at.% Lu^{3+} and 10.8 at.% Lu^{3+}, ***a***-cut crystal, T_{OC} = 1.5%.

deteriorated: the laser threshold increased from 1.22 W to 2.17 W, the slope efficiency slightly decreased from 8.6% to 8.5% and the maximum output power dropped from 250 mW to 198 mW. A similar trend was also observed for samples oriented for light propagation along the ***c***-axis, cf. Table 2. These changes indicate increased scattering losses in the crystal containing 10.8 at.% Lu^{3+}. For both studied crystals, the thermal roll-over in the input-output dependences was observed approximately in the same range of absorbed pump powers. No crystal fracture was observed up to at least P_{abs} = 5.1 W. Thus, the decrease of thermal

conductivity of Tm,Ho:Ca(Gd,Lu)AlO_4 crystals when increasing the Lu^{3+} content from 5.5 at.% to 10.8 at.% is relatively weak.

5. Conclusions

To conclude, $CaGdAlO_4$ crystals codoped with buffer Lu^{3+} ions and laser-active Tm^{3+} and Ho^{3+} ions resulting in a complex solid solution in the Ca ($Ln1_{1-x-y-z}Ln2_xLn3_yLn4_z$)$AlO_4$ system are attractive gain materials for broadly tunable and mode-locked lasers emitting in the eye-safe spectral range of ~2 μm. This is because of the following spectroscopic features revealed in this work: (i) a significant inhomogeneous broadening of the spectral bands, induced both by the structure and compositional disorder, (ii) a strong polarization-anisotropy of stimulated-emission properties for Ho^{3+} ions, (iii) an efficient and predominantly unidirectional $Tm^{3+} \rightarrow Ho^{3+}$ energy transfer, expressed by the equilibrium constant $\Theta = 0.064$, and (iv) broad and smooth gain spectra (gain bandwidth: about 100 nm) for σ-polarization extending well above 2 μm thus avoiding the unwanted structured water vapor absorption in the atmosphere. In addition, the crystals exhibit good thermo-optic behavior as indicated by diode-pumped laser operation in true CW regime.

We also present a spectroscopic evidence of the effect of Lu^{3+} codoping on the emission properties of active ions (in particular, Ho^{3+} ones) being more significant for σ-polarization which is particularly attractive for ML applications. The study of crystals with higher Lu^{3+} doping levels (note that the upper limit of the existence of the $CaGd_{1-x}Lu_xAlO_4$ solid solution is not yet known) is thus very promising.

During the revision process of this manuscript, we have achieved passive mode-locking of a Tm,Ho:Ca(Gd,Lu)AlO_4 laser using a crystal with 5.5 at.% Lu^{3+} resulting in generation of pulses as short as 46 fs at 2033 nm with an average power of 121 mW at a pulse repetition rate of ~78 MHz employing a semiconductor saturable absorber mirror [37]. To the best of our knowledge, this result represents the shortest pulses ever generated from any Tm- and/or Ho-based aluminate solid-state laser. This laser result confirms the conclusions about the positive role of Lu^{3+} addition on boosting the broadband emission properties of Tm, Ho:$CaGdAlO_4$ crystals.

Further power scaling and reduction of the heat loading in the Tm, Ho:Ca(Gd,Lu)AlO_4 lasers seems feasible under in-band pumping (directly to the Tm^{3+} upper laser level, $^3F_4$), e.g., by using Erbium Raman fiber lasers [38].

Credit author statement

Zhongben Pan: Investigation, **Pavel Loiko:** Conceptualization, Writing – original draft, Investigation, **Josep Maria Serres:** Investigation, Writing – original draft, **Hualei Yuan:** Investigation, **Yicheng Wang:** Investigation, **Li Wang:** Investigation, **Yongguang Zhao:** Investigation, **Rosa Maria Solé:** Data curation, Investigation, **Magdalena Aguiló:** Funding acquisition, Supervision **Francesc Díaz:** Funding acquisition, **Patrice Camy:** Supervision, **Weidong Chen:** Writing – original draft, **Uwe Grieber:** Supervision, **Valentin Petrov:** Writing – review & editing, **Xavier Mateos:** Conceptualization, Writing – review & editing, Investigation.

Declaration of competing interest

The authors declare that they have no known competing financial interests or personal relationships that could have appeared to influence the work reported in this paper.

Acknowledgements

This work was possible thanks to Grant PID2019-108543RB-I00 funded by MCIN/AEI/ 10.13039/501100011033 and by the Generalitat de Catalunya (project No. 2017SGR755). National Natural Science Foundation of China (52072351), China Academy of Engineering Physics (CAEP) (YZJJLX2018005), Fund of Key Laboratory of Optoelectronic Materials Chemistry and Physics, Chinese Academy of Sciences (2008DP173016).

References

[1] K. Scholle, S. Lamrini, P. Koopmann, P. Fuhrberg, 2 μm laser sources and their possible applications, in: B. Pal (Ed.), Frontiers in Guided Wave Optics and Optoelectronics, Intech, 2010, pp. 471–500.
[2] U.N. Singh, B.M. Walsh, J. Yu, M. Petros, M.J. Kavaya, T.F. Refaat, N.P. Barnes, Twenty years of Tm:Ho:YLF and LuLiF laser development for global wind and carbon dioxide active remote sensing, Opt. Mater. Express 5 (2015) 827–837.
[3] T.A. Wollin, J.D. Denstedt, The holmium laser in urology, J. Clin. Laser Med. Surg. 16 (1998) 13–20.
[4] S. Lamrini, P. Koopmann, M. Schäfer, K. Scholle, P. Fuhrberg, Directly diode-pumped high-energy Ho:YAG oscillator, Opt. Lett. 37 (2012) 515–517.
[5] P.A. Budni, L.A. Pomeranz, M.L. Lemons, C.A. Miller, J.R. Mosto, E.P. Chicklis, Efficient mid-infrared laser using 1.9-μm-pumped Ho:YAG and $ZnGeP_2$ optical parametric oscillators, J. Opt. Soc. Am. B 17 (2000) 723–728.
[6] T.Y. Fan, G. Huber, R.L. Byer, P. Mitzscherlich, Spectroscopy and diode laser-pumped operation of Tm,Ho:YAG, IEEE J. Quant. Electron. 24 (1988) 924–933.
[7] G.L. Bourdet, G. Lescroart, Theoretical modeling and design of a Tm,Ho:$YLiF_4$ microchip laser, Appl. Opt. 38 (1999) 3275–3281.
[8] P. Loiko, J.M. Serres, X. Mateos, K. Yumashev, N. Kuleshov, V. Petrov, U. Griebner, M. Aguiló, F. Díaz, Microchip laser operation of Tm,Ho:$KLu(WO_4)_2$ crystal, Opt Express 22 (2014) 27976–27984.
[9] B.M. Walsh, N.P. Barnes, B. Di Bartolo, The temperature dependence of energy transfer between the Tm $^3F_4$ and Ho $^5I_7$ manifolds of Tm-sensitized Ho luminescence in YAG and YLF, J. Lumin. 90 (2020) 39–48.
[10] I.F. Elder, M.J.P. Payne, Lasing in diode-pumped Tm:YAP, Tm,Ho:YAP and Tm,Ho:YLF, Opt Commun. 145 (1998) 329–339.
[11] Y. Zhao, Y. Wang, X. Zhang, X. Mateos, Z. Pan, P. Loiko, W. Zhou, X. Xu, J. Xu, D. Shen, S. Suomalainen, A. Härkönen, M. Guina, U. Griebner, V. Petrov, 87 fs mode-locked Tm,Ho:$CaYAlO_4$ laser at ~2043 nm, Opt. Lett. 43 (2018) 915–918.
[12] Z. Pan, Y. Wang, Y. Zhao, M. Kowalczyk, J. Sotor, H. Yuan, Y. Zhang, X. Dai, H. Cai, J.E. Bae, S.Y. Choi, F. Rotermund, P. Loiko, J.M. Serres, X. Mateos, U. Griebner, V. Petrov, Sub-80 fs mode-locked Tm,Ho-codoped disordered garnet crystal oscillator operating at 2081 nm, Opt. Lett. 43 (2018) 5154–5157.
[13] Y. Zhao, Y. Wang, W. Chen, Z. Pan, L. Wang, X. Dai, H. Yuan, Y. Zhang, H. Cai, J. E. Bae, S.Y. Choi, F. Rotermund, P. Loiko, J.M. Serres, X. Mateos, W. Zhou, D. Shen, U. Griebner, V. Petrov, 67-fs pulse generation from a mode-locked Tm,Ho:CLNGG laser at 2083 nm, Opt Express 27 (2019) 1922–1928.
[14] Y. Wang, G. Xie, X. Xu, J. Di, Z. Qin, S. Suomalainen, M. Guina, A. Härkönen, A. Agnesi, U. Griebner, X. Mateos, P. Loiko, V. Petrov, SESAM mode-locked Tm:CALGO laser at 2 μm, Opt. Mater. Express 6 (2016) 131–136.
[15] J. Di, X. Xu, C. Xia, Q. Sai, D. Zhou, Z. Lv, J. Xu, Growth and spectra properties of Tm, Ho doped and Tm, Ho co-doped $CaGdAlO_4$ crystals, J. Lumin. 155 (2014) 101–107.
[16] R. Moncorgé, N. Garnier, P. Kerbrat, C. Wyon, C. Borel, Spectroscopic investigation and two-micron laser performance of Tm^{3+}:$CaYAlO_4$ single crystals, Opt Commun. 141 (1997) 29–34.
[17] W. Yao, F. Wu, Y. Zhao, H. Chen, X. Xu, D. Shen, Highly efficient Tm:$CaYAlO_4$ laser inband pumped by a Raman fiber laser at 1.7 μm, Appl. Opt. 55 (2016) 3730–3733.
[18] D. Zhou, J. Di, C. Xia, X. Xu, F. Wu, J. Xu, D. Shen, T. Zhao, A. Strzęp, W. Ryba-Romanowski, R. Lisiecki, Spectroscopy and laser operation of Ho:$CaYAlO_4$, Opt. Mater. Express 3 (2013) 339–345.
[19] L. Vasylechko, N. Kodama, A. Matkovskii, Y. Zhydachevskii, Crystal structure and optical spectroscopy of $CaGdAlO_4$:Er single crystal, J. Alloys Compd. 300 (2000) 475–478.
[20] P.O. Petit, J. Petit, P. Goldner, B. Viana, Inhomogeneous broadening of optical transitions in Yb:$CaYAlO_4$, Opt. Mater. 30 (2008) 1093–1097.
[21] P. Loiko, F. Druon, P. Georges, B. Viana, K. Yumashev, Thermo-optic characterization of Yb:$CaGdAlO_4$ laser crystal, Opt. Mater. Express 4 (2014) 2241–2249.
[22] S. Gao, Z. You, J. Xu, Y. Sun, C. Tu, Continuous wave laser operation of Tm and Ho co-doped $CaYAlO_4$ and $CaGdAlO_4$ crystals, Mater. Lett. 141 (2015) 59–62.
[23] Q. Hu, Z. Jia, A. Volpi, S. Veronesi, M. Tonelli, X. Tao, Crystal growth and spectral broadening of a promising Yb:$CaLu_xGd_{1-x}AlO_4$ disordered crystal for ultrafast laser application, CrystEngComm 19 (2017) 1643–1647.
[24] Z. Pan, P. Loiko, J.M. Serres, E. Kifle, H. Yuan, X. Dai, H. Cai, Y. Wang, Y. Zhao, M. Aguiló, F. Díaz, U. Griebner, V. Petrov, X. Mateos, Mixed" Tm:Ca(Gd,Lu)AlO_4 — a novel crystal for tunable and mode-locked 2 μm lasers, Opt Express 27 (2019) 9987–9995.
[25] Z. Pan, P. Loiko, S. Slimi, H. Yuan, X. Dai, H. Cai, Y. Wang, Y. Zhao, P. Camy, E. Dunina, A. Kornienko, L. Fomicheva, W. Chen, U. Griebner, V. Petrov, R. Solé, F. Díaz, M. Aguiló, X. Mateos, Tm,Ho:Ca(Gd,Lu)AlO_4 crystals: Crystal growth, structure refinement and Judd-Ofelt analysis, J. Lumin. (2021) *submitted to*.
[26] A.E. Troshin, V.E. Kisel, A.S. Yasukevich, N.V. Kuleshov, A.A. Pavlyuk, E. B. Dunina, A.A. Kornienko, Spectroscopy and laser properties of Tm^{3+}:$KY(WO_4)_2$ crystal, Appl. Phys. B 86 (2007) 287–292.
[27] P. Loiko, P. Becker, L. Bohatý, C. Liebald, M. Peltz, S. Vernay, D. Rytz, J.M. Serres, X. Mateos, Y. Wang, X. Xu, J. Xu, A. Major, A. Baranov, U. Griebner, V. Petrov, Sellmeier equations, group velocity dispersion and thermo-optic dispersion

formulas for $CaLnAlO_4$ (Ln =Y, Gd) laser host crystals, Opt. Lett. 42 (2017) 2275–2278.
[28] B.M. Walsh, N.P. Barnes, B. Di Bartolo, On the distribution of energy between the Tm $^3F_4$ and Ho $^5I_7$ manifolds in Tm-sensitized Ho luminescence, J. Lumin. 75 (1997) 89–98.
[29] S. Li, Y. Yang, S. Zhang, T. Yan, N. Ye, Y. Hang, Enhanced 2.86 μm emission from a Ho,Pr:$CaGdAlO_4$ crystal, J. Lumin. 228 (2020), 117620.
[30] E. Kifle, P. Loiko, C. Romero, J.R.V. de Aldana, V. Zakharov, Y. Gurova, A. Veniaminov, V. Petrov, U. Griebner, R. Thouroude, M. Laroche, P. Camy, M. Aguiló, F. Díaz, X. Mateos, Tm^{3+} and Ho^{3+} colasing in in-band pumped waveguides fabricated by femtosecond laser writing, Opt. Lett. 46 (2021) 122–125.
[31] S. Kurilchik, N. Gusakova, M. Demesh, A. Yasukevich, V. Kisel, A. Pavlyuk, N. Kuleshov, Energy transfer in Tm,Ho:KYW crystal and diode-pumped microchip laser operation, Opt Express 24 (2016) 6451–6458.
[32] J.A. Hutchinson, H.R. Verdun, B.H. Chai, B. Zandi, L.D. Merkle, Spectroscopic evaluation of $CaYAlO_4$ doped with trivalent Er, Tm, Yb and Ho for eyesafe laser applications, Opt. Mater. 3 (1994) 287–306.
[33] B. Aull, H. Jenssen, Vibronic interactions in Nd:YAG resulting in nonreciprocity of absorption and stimulated emission cross sections, IEEE J. Quant. Electron. 18 (1982) 925–930.
[34] S.A. Payne, L.L. Chase, L.K. Smith, W.L. Kway, W.F. Krupke, Infrared cross-section measurements for crystals doped with Er^{3+}, Tm^{3+} and Ho^{3+}, IEEE J. Quant. Electron. 28 (1992) 2619–2630.
[35] Z. Pan, P. Loiko, Y. Wang, Y. Zhao, H. Yuan, X. Dai, H. Cai, J.M. Serres, S. Slimi, E. Dunina, A. Kornienko, J.-L. Doualan, P. Camy, U. Griebner, V. Petrov, M. Aguiló, F. Díaz, X. Mateos, Disordered Tm^{3+},Ho^{3+}-codoped CNGG garnet crystal: towards efficient laser materials for ultrashort pulse generation at ~2 μm, J. Alloys Compd. 853 (2021), 157100, 157101-15.
[36] P. Loiko, J.M. Serres, X. Mateos, X. Xu, J. Xu, V. Jambunathan, P. Navratil, A. Lucianetti, T. Mocek, X. Zhang, U. Griebner, V. Petrov, M. Aguiló, F. Díaz, A. Major, Microchip Yb:$CaLnAlO_4$ lasers with up to 91% slope efficiency, Opt. Lett. 42 (2017) 2431–2434.
[37] L. Wang, W. Chen, Y. Zhao, P. Loiko, X. Mateos, M. Guina, Z. Pan, M. Mero, U. Griebner, V. Petrov, Sub-50 fs pulse generation from a SESAM mode-locked Tm, Ho-codoped calcium aluminate laser, Opt. Lett. 46 (2021) 2642–2645.
[38] P. Loiko, R. Thouroude, R. Soulard, L. Guillemot, G. Brasse, B. Guichardaz, A. Braud, A. Hideur, M. Laroche, H. Gilles, P. Camy, In-band pumping of Tm:$LiYF_4$ channel waveguide: a power scaling strategy for ~2 μm waveguide lasers, Opt. Lett. 44 (2019) 3010–3013.